Design of a novel three- dimensional-printed two degrees-of-freedom steerable electrosurgical grasper for minimally invasive surgery

Sakes, Aimée; Hovland , Kevin; Smit, Gerwin; Geraedts, Jo; Breedveld, Paul

DOI
10.1115/1.4038561

Publication date
2018

Document Version
Final published version

Published in
Journal of Medical Devices

Aimée Sakes[1]
Department BioMechanical Engineering,
Faculty Mechanical, Maritime,
and Materials Engineering,
Delft University of Technology,
Mekelweg 2,
Delft 2628 CD, The Netherlands
e-mail: a.sakes@tudelft.nl

Kevin Hovland
Department BioMechanical Engineering,
Faculty Mechanical, Maritime,
and Materials Engineering,
Delft University of Technology,
Mekelweg 2,
Delft 2628 CD, The Netherlands
e-mail: tigermeet@live.nl

Gerwin Smit
Department BioMechanical Engineering,
Faculty Mechanical, Maritime,
and Materials Engineering,
Delft University of Technology,
Mekelweg 2,
Delft 2628 CD, The Netherlands
e-mail: g.smit@tudelft.nl

Jo Geraedts
Department Design Engineering,
Faculty Industrial Design Engineering,
Delft University of Technology,
Mekelweg 2,
Delft 2628 CD, The Netherlands
e-mail: j.m.p.geraedts@tudelft.nl

Paul Breedveld
Department BioMechanical Engineering,
Faculty Mechanical, Maritime,
and Materials Engineering,
Delft University of Technology,
Mekelweg 2,
Delft 2628 CD, The Netherlands
e-mail: p.breedveld@tudelft.nl

Design of a Novel Three-Dimensional-Printed Two Degrees-of-Freedom Steerable Electrosurgical Grasper for Minimally Invasive Surgery

In current bipolar electrosurgical instruments, a high frequency electrical sinusoidal wave is passed through the patient's body from an active electrode to the return electrode to cut, coagulate, or desiccate tissues. Even though current bipolar electrosurgical instruments have proven effective in minimizing blood loss, advancement is needed to allow for improved dexterity and adaptability. With current advances in three-dimensional (3D)-print processes and its integration in the medical field, it has become possible to manufacture patient-and operation-specific instruments. In this study, we introduce the first 3D-printed steerable bipolar grasper (□ 5 mm) for use in minimal invasive surgery. The grasper significantly improves dexterity by the addition of two planar joints allowing for ±65 deg for sideways and ±85 deg for up- and downward movement. The joints enable a significantly higher bending stiffness, 4.0 N/mm for joint 1 and 4.4 N/mm for joint 2, than that of currently available steerable instruments. The tip consists of two metallic movable jaws that can be opened and closed with angles up to 170 deg and allows for grasping and coagulating of tissues; reaching tissue temperatures of over 75 °C for an activation time of ∼5 s, respectively. In order to actuate the joint, tip, and electrosurgical system, as well as to tension the steering cables, a ring handle was designed. In summary, the 3D-printed steerable bipolar grasper provides the surgeon with electrosurgical capabilities, improved dexterity, improved stiffness, and the versatility that is needed to provide patient- and operation-specific care.
[DOI: 10.1115/1.4038561]

Keywords: 3D-printing, additive manufacturing, bipolar electrosurgery, medical device design, minimally invasive surgery, steerable instruments

1 Introduction

Controlling blood loss is a major challenge in open and minimally invasive surgery (MIS) [1]. Even though the human body has a unique process that stops blood loss after an injury called hemostasis, this process is often too slow or insufficient to stop major bleeding. In order to accelerate the process of hemostasis during MIS, electrosurgery is often used. In electrosurgery, a high frequency (0.3–5 MHz) electrical sinusoidal wave is passed through the patient's body from an active electrode to a return electrode in order to coagulate, cut, or desiccate the target tissue between the electrodes. The effect is determined by the waveform, voltage, and power of the electrosurgical current, as well as the size of electrode tip. The tissue between the electrodes is damaged due to the conversion of the electrical energy of the alternating current into heat. As the water evaporates, tissue fragmentation occurs and the electrode can coagulate or cut straight through the tissue [1].

Even though electrosurgical tools have proven effective in minimizing blood loss, advancement is needed to allow for a higher tool reach and for more adaptable devices that are both patient- and operation-specific. Currently, clinically available bipolar electrosurgical tools, such as *Endopath* (Ethicon, Somerville, NJ) [2] and *Aesculap PM438R* (B. Braun Medical B.V., Oss, The Netherlands) [3], are rigid and are thus only able to rotate around, and slide through, the incision point (or trocar). This restricts these instruments to four degrees-of-freedom (4 DOF)—axial translation/sliding, axial rotation, and radial rotation in two planes (Fig. 1 left)—and thus does not allow for reaching around tissues or changing the orientation of the tip of the instrument with respect to the shaft.

In order to improve the reach of the tool, it is necessary to increase the DOF of the tip portion by adding a steerable section (or wrist joint; Fig. 1 right), such as in the Da Vinci wristed robotic electro-cautery instruments [4]. Furthermore, as each patient and each operation is different, currently available rigid

[1]Corresponding author.
Manuscript received June 19, 2017; final manuscript received November 1, 2017; published online January 10, 2018. Assoc. Editor: Venketesh Dubey.

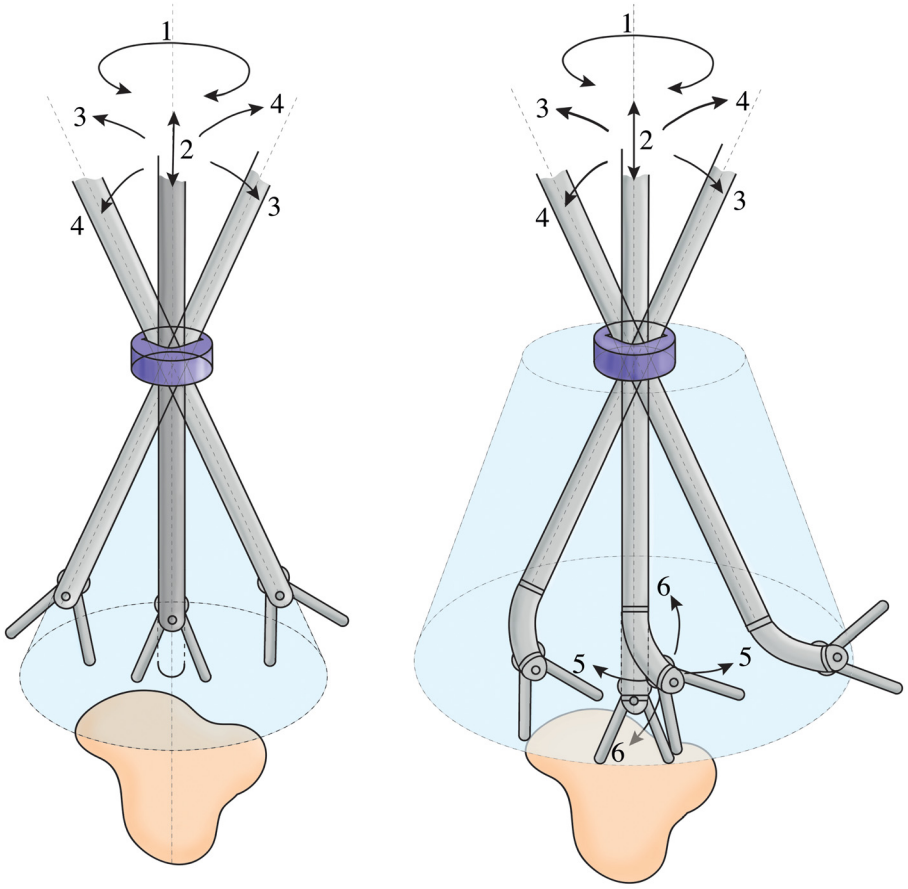

Fig. 1 Degrees-of-freedom and workspace of bipolar electrosurgical tools. Left: DOF of currently clinical available electrosurgical tools. Right: DOF of the proposed minimally invasive bipolar electrosurgical instrument. Number indications: 1: axial rotation, 2: axial translation or sliding, 3 and 4: radial rotation or pivoting in two perpendicular planes, 5: pivoting of the instrument tip, and 6: pivoting of the instrument tip in a perpendicular plane to 5.

instruments are suboptimal. Even though there are bipolar electrosurgical tools with different tip sections available, there are only a limited amount of options when it comes to shaft size and shape. Easily adaptable, patient-specific tools are needed to increase the efficiency and ease of MIS procedures, such as in skull base and arthroscopic procedures in which tight spaces need to be navigated. With current advances in three-dimensional (3D) printing and its integration with the medical field, it has become possible to manufacture patient-specific tools on an on-demand basis. The goal of this study is, therefore, to design and validate a steerable 3D-printed adaptable bipolar grasper for use in electrosurgery to improve upon the workspace of current rigid electrosurgical tools and to allow for an adaptable, patient-and/or operation-specific tool.

2 Design Requirements

2.1 Tip Requirements. At the distal end of the instrument, a grasper should be placed to grip, manipulate, and coagulate tissues. The tip should consist of two movable electrical jaws that are able to grasp tissues in between the jaws, similar to currently available minimally invasive graspers (Fig. 2). Each jaw should be provided with a profile to improve the grip on slippery tissues (Fig. 2). The jaws should open to an angle of at least 60 deg (Fig. 2), which is comparable to instruments currently used in clinical practice [5,6]. Furthermore, the joint that opens and closes the jaws/gripper should be placed in close proximity to the steering joint(s) to increase the control accuracy of the tip. Additionally, the electrical resistivity of the tip material should be lower than 1.8×10^{-6} Ωm, which is in the range of metals [7], to allow for proper conduction of the electric signal. Finally, the thermal capacity of the tip should be higher than 0.1 J/kgK to prevent the tip from heating up when the current is applied.

2.2 Steerability Requirements. As previously discussed, rigid minimally invasive instruments allow for 4 DOF motion around the incision point (the trocar; Fig. 1 right). This limited

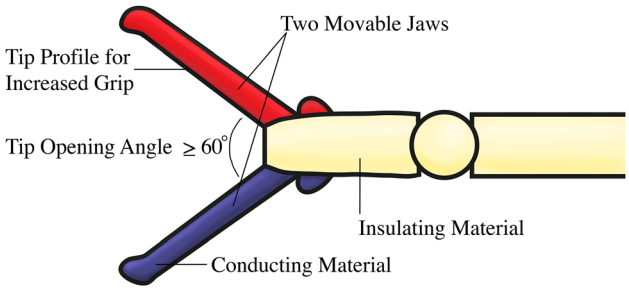

Fig. 2 Tip requirements of the proposed minimally invasive bipolar electrosurgical instrument. The tip should contain two movable jaws out of a conducting material with a tip profile to increase grip on the tissue. The movable jaws should open up to at least 60 deg. An insulating layer separates the two movable jaws.

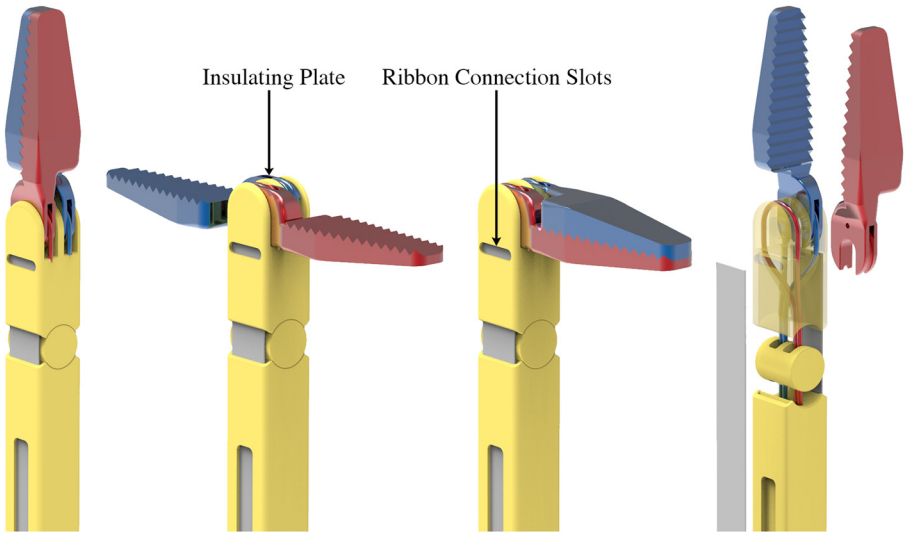

Fig. 3 Final tip design working principle. Left: tip in the closed (0 deg) configuration with the tip joint in the minimum curve angle (straight: 0 deg). An insulating plate is present to prevent short-circuiting the instrument. Middle: tip in the open (180 deg) configuration with the tip joint in the minimum curve angle (straight: 0 deg). Right: tip in the closed (0 deg) configuration with the tip joint in the maximum curve angle (±90 deg). The steering ribbon for the more proximal joint is connected to the shaft between the joints using a hook.

number of DOF greatly restricts the range of motion of the surgeon. To improve the reach of the tool and to allow the surgeon to change the tip orientation (to improve positioning), 2DOF of bending motion were added to the instrument (Fig. 1 right). The bending angle for the steering joint should be equal to or higher than 60 deg to significantly increase the reach of the tool. Furthermore, the joint should have both a high torsional stiffness to resist twisting/rotation of the joint around the axial axis and a high bending stiffness to resist unwanted bending motion caused by lateral forces. In a study published by Jelínek et al. [8], the bending stiffnesses of three steerable instruments—*DragonFlex* (2DOF, □ 5 mm, 3D-printed, Delft University of Technology, Delft, The Netherlands), *Miflex* (2DOF, Ø5 mm, Deam Corporation, Amsterdam, The Netherlands), and *Laparo-Angle* (3DOF, Ø5 mm, Cambridge Endo, Framingham, MA)—were evaluated for different bending angles. The bending stiffness ranged from 0.56 N/mm for Laparo-Angle in a straight configuration up to 2.94 N/mm for Miflex with a bending angle of 60 deg, with the Dragonflex performing most consistently over all bending angles with an overall bending stiffness of around 2 N/mm. Therefore, a bending stiffness of at least 0.56 N/mm is preferred. Unfortunately, no data is available about the torsional stiffness of currently available steerable MIS instruments.

2.3 Shaft Requirements. Between the steerable joint and handle of the instrument, a rigid shaft should be placed. The maximum diameter of the shaft is set to 7 mm, which is in the range of conventional laparoscopic instruments [5,9,10] and can be used in most procedures. The shape and length of the prototype should be easily adjustable, in order to allow for a patient- and operation-specific tool that can be used to perform MIS in different parts of the body. Similar to the steerable joint, the shaft of the instrument should have high torsional and bending stiffness. Furthermore, the shaft should contain multiple lumens to guide the active and return electrodes from the tip toward the handle. Finally, the shaft should be made out of a material with a high thermal capacity ($\geq$1 J/kgK) and electrical resistivity ($\geq 1 \times 10^{12}$ Ωm)—which is similar to common insulators—in order to prevent heating and current leakage from the instrument [7].

2.4 Handle Requirements. The instrument should allow for single-handed control. The handle should allow the operator to steer the joint(s), open and close the jaws, and connect the instrument to an electrosurgical unit.

2.5 Electrical Circuit Requirements. In general, the frequencies of the waves used in electrosurgery lie between 300 kHz and 5 MHz and the power between 15 and 500 W [1,11]. Hence, the instrument needs to be able to support these power settings when connected to an electrosurgical unit. For this purpose, the electrodes should be made out of a material with a low electrical resistivity ($\leq 1.2 \times 10^{-6}$ Ωm), which is similar to common metals [7]. Furthermore, similar to the shaft, the electrodes should also have a high thermal capacity ($\geq$1 J/kgK) to prevent heating.

3 Steerable Bipolar Grasper Design

3.1 Tip and Joint Design. In Appendix, we describe the fundamental joint categorization, in which we explain the joint types and ways of guiding the electrical current through or around the joint, the selection process of the joint design, and the joint optimization protocol. In Fig. 3, the final tip and joint design is illustrated. At the distal tip of the instrument, the two movable jaws are made out of a metallic, conductive material and form the active and return electrode of the instrument (Fig. 3). A triangular profile (90 deg top angle, 1 mm high) is added to the grasping surfaces to increase the grip on the tissue. The tip jaws are insulated from each other (with the exception of the grasping surfaces) by a nonconducting polymeric plate in the middle of the joint to prevent short circuits (Fig. 3). The tip jaws are connected to a fixed, nonconducting polymeric axle embedded into the joint. Two nonconducting polymeric outer plates are placed at the outer edge of the joint to provide support to the axle and prevent the tip jaws from sliding sideways (Fig. 3). The up- and downward movement and the opening and closing of the tip jaws are controlled by two electrode cables that are looped around each of the tip jaws (Fig. 3). The maximum opening angle of the two movable jaws and curve angle of the joint is 180 deg (90 deg in each

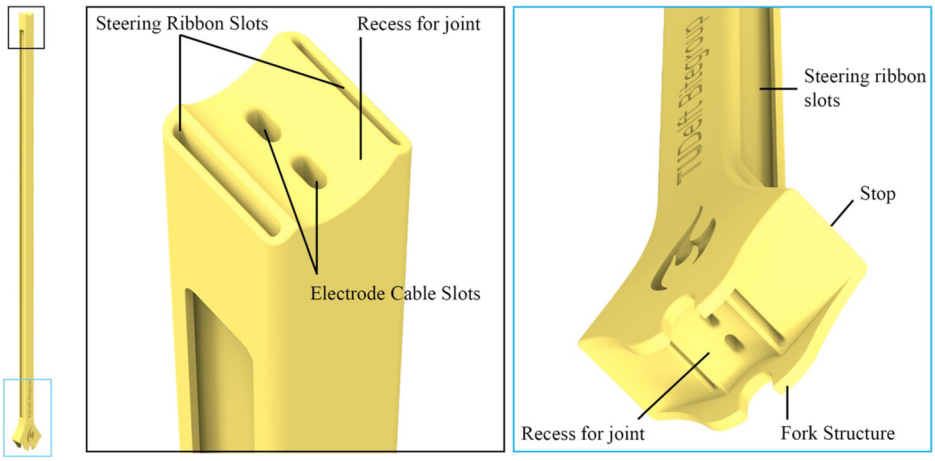

Fig. 4 Final shaft design. Left: total shaft design. Middle: distal end of shaft with the rounded rectangular lumens for the electrode cables and steering ribbons and the cylindrical recess for the planar joint. Right: proximal end of shaft with the rounded rectangular lumens for the electrode cables and steering ribbons, the cylindrical recess for mirrored planar joint, two fork structures to increase the stability of the joint, and stops to prevent over-bending the joints.

direction; Fig. 3). Finally, two steering ribbons actuate the first planar joint that allows for sideways deflections of ±65 deg. The steering ribbons are guided through rectangular slots in the connecting element between the two joints and are fixed by injecting an adhesive into the slot (Fig. 3). Inside the cylindrical planar joint, curved slots ($r = 2.5$ mm; 5.5x electrode cable diameter) are present to guide the electrode steering cables toward the shaft and prevent cable fatigue.

The unique design of both joints, specifically the use of a ribbon to control the joint, has two main advantages. First, the ribbon and cables are placed at the outer edge of the joint, which increases the moment arms and thus reduces the force required to bend the tip, while at the same time increasing the bending stiffness of the joint. For comparison, if a similar cross-sectional area cable was used with a diameter of 0.6 mm (2x thicker than the ribbon), the moment arms would have been reduced with approximately 7%. Second, due to the minimal thickness of the ribbon, it can accommodate small curve radii (0.4 mm in the grasper) without suffering from cable fatigue, allowing for navigating through tight curves.

3.2 Shaft and Handle Design. The shaft connects the joint and tip of the instrument with the handle. The shaft has a rectangular shape (□ 5 mm, $l = 150$ mm). Note that the shaft length, shape (straight versus curved), and size can be easily adapted and, subsequently, 3D-printed, to allow for a patient- and operation-specific grasper. This way, differences in body mass and lengths of patients, for example, can be accounted for. Furthermore, depending on the type of MIS procedure, different shaft shapes, including curved shafts, can come in handy, for example, when navigating through tight spaces. In order to achieve these patient-specific tools, a 3D computer-aided design (CAD) model of the instrument in combination with patient data obtained from a pre-operative computed tomography or magnetic resonance imaging scan could be used.

The electrode cables run through two rounded rectangular lumens in the center of the shaft, while the steering ribbons are guided through rectangular slots near the surface of the shaft (Fig. 4). At the distal and proximal end of the shaft, two identical cylindrical recesses are present in which the two (mirrored) planar joints are contained (Fig. 4).

The handle allows for single-handed control of the two tip joints, the movable tip jaws, and the electrical circuit. To steer the instrument in 2DOF and control the tip jaws, the joint structure of the tip is mirrored in the handle (Fig. 5). A similar approach is seen in the 3D-printed Dragonflex device [12]. The joints are similar to those situated in the tip, with a few exceptions. (1) In order to keep the steering ribbons under tension, two equal tension mechanisms have been added to the connecting element between the two joints (Fig. 5). The tension mechanisms consist of a rectangular metallic cube with a rectangular lumen through which the steering ribbons are guided and an M2 set screw to fix the steering ribbon in place. (2) The electrode cables are guided through two separate rectangular lumens running from the apex of the second planar joint groove toward and through the ring handle parts, instead of being looped around the joint (Fig. 5). In this way, by moving, opening, or closing the ring handle parts, the jaws will rotate, open, or close, respectively. Furthermore, in order to keep the electrode cables tensioned, two identical cable-tensioning mechanisms have been added to the ring handle parts, one for each tip jaw (Fig. 5). The cable tensioning mechanism consists of a cylindrical tension knob screwed onto a square head M2 full-threaded bolt that is placed within a square recess in the ring handle (Fig. 5). Inside the M2 screw, a lumen (Ø1 mm) is present through which the electrode cables are guided. To fix the cables to the tensioning mechanisms, a small knot was made at the distal end of the cables, and the lumens were filled with an adhesive. By rotating the knob, the screw will translate left or right (depending on the rotation direction) and, as such, will tension or release the electrode cables, respectively. (3) To increase the stability of the joints and prevent the first joint from sliding sideways, two cylindrical protrusions and two outer plates that grip around the protrusions have been added to the joints themselves, the shaft, and the connecting element between the joints (Fig. 5), respectively. (4) Furthermore, stops have been added to the shaft, the connection element between the joints, and the ring handles to prevent damage to the joints and cables due to excessive bending (Fig. 5). Finally, to connect an electrosurgical unit to the instrument, two fittings have been added to the ring handles (Fig. 5). In Fig. 6, the complete final design is illustrated.

4 Prototype Development

4.1 Three-Dimensional-Printing Process and Material Selection. Material selection is an important aspect of the design process to allow for proper electrical conductivity and heat capacity in both the conductive and insulating parts of the instrument. In Table 1, an overview is given of the selected

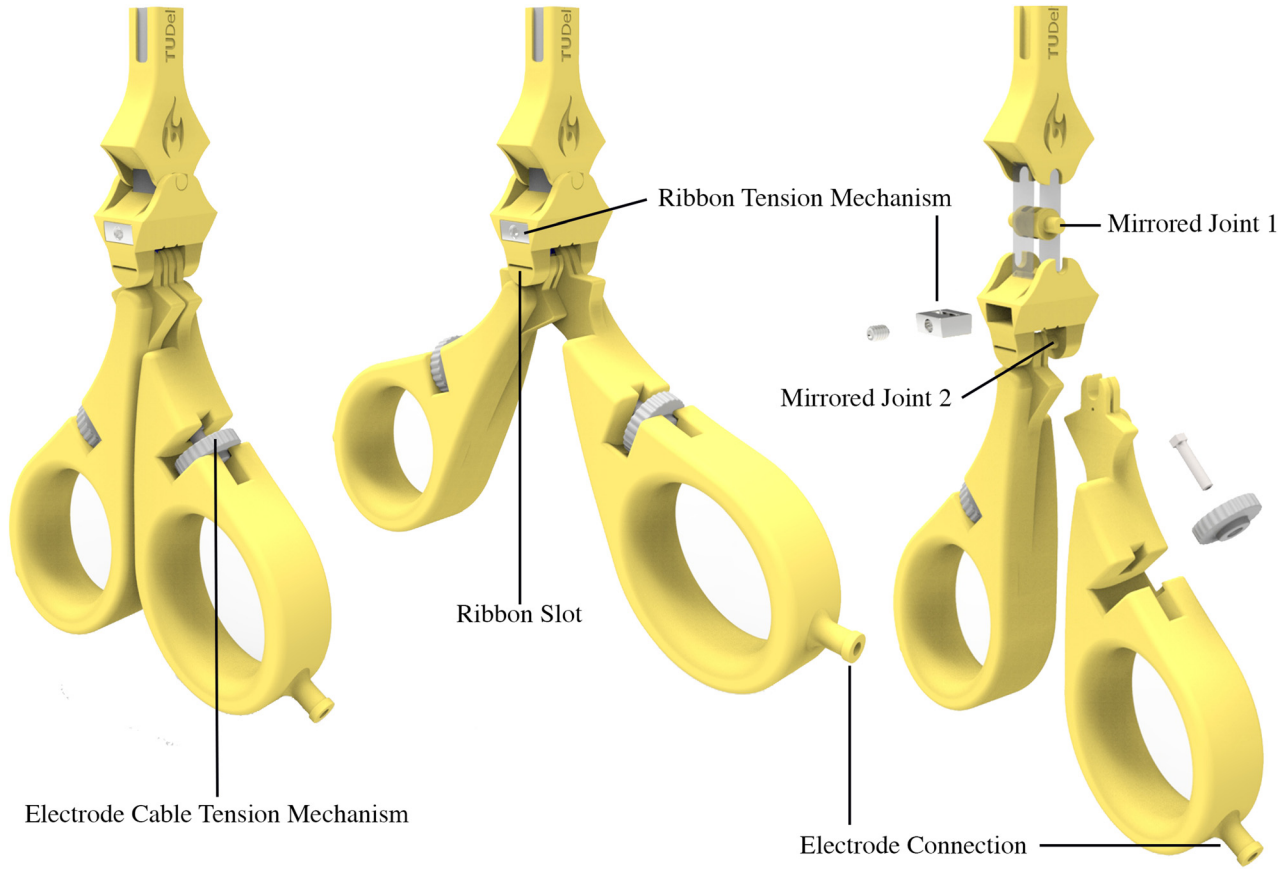

Fig. 5 Final handle design. The handle allows for steering the two joints by mirroring the joint in the handle, opening and closing of the tip jaws, tensioning the steering ribbons and electrode cables, and connecting the electrosurgical unit. Left: total handle design in the closed configuration. Middle: Handle in the open configuration. Right; exploded view of the handle.

3D-printable materials and their material properties. At an early stage of the design process, more 3D-printable materials were considered. However, another factor that was taken into account was the resolution of the printer, which was often insufficient for our purposes. Therefore, for the polymeric parts (joints, shaft, and handle), we decided to use the *Perfactory 4 Standard* (EnvisionTec GmbH, Gladbeck, Germany) 3D-printer, which allows for high accuracy part manufacturing (with a resolution of 100 μm, 100 μm, and 15–150 μm in the x, y, and z directions, respectively) [13]. The material used for our prototype is R5 red, a liquid photopolymer that produces robust, accurate, and functional parts with a flexural modulus of 1190–1383 MPa and tensile strength of 31–39 MPa [14]. Unfortunately, the thermal capacity and electrical resistivity are untested for this polymer. We, therefore, experimentally determined these variables. To determine the thermal capacity, a heat element (*HM6800*, Minco, Minneapolis, MN) connected to the R5 test rod and a power unit (*ES 030-5*, Delta Elektronika, Zierikzee, The Netherlands; controlled and measured by NI USB-6008, National Instruments, Woerden, The Netherlands) were placed inside an insulated box (220 mm $\times$ 200 mm $\times$ 120 mm; $l \times w \times h$). The thermal capacity was measured using four thermocouples (NI 9211 in combination with NI USB-9162, National Instruments, Woerden, The Netherlands): one for the outside temperature, one for the inside temperature, one for the heat element, and one for the R5 test rod. Three consecutive tests were performed. Based on these tests, the thermal capacity was estimated as 1182 ± 69 J/kgK ($m = 0.00428$ kg), which is sufficient for our application. The electrical resistivity of the material was determined by connecting an electrometer (*6517A*, Keithley, Beaverton, OR) to the R5 test rod. A value of $\geq 1.67 \times 10^{18}$ Ωm was determined ($R \geq 1 \times 10^{15}$ Ω, $A = 90 \times 10^{-6}$ m^2, and $L = 0.15$ m), which is again sufficient for our application.

For the metal tip jaws, the *SLM 125* (ReaLizer GmbH, Borchen, Germany; using an exposure time of 20 μs, point distance of 10 μm, and laser current of 1100 mA) 3D-printer was used as this printer allows for high-precision printing (with a resolution of 20–100 μm in the x, y, and z directions) of the biocompatible titanium alloy Ti6Al4V [15]. Ti6Al4V has a Young's modulus of 113.8 GPa, ultimate tensile strength of 950 Mpa, electrical resistivity of 1.8×10^{-6} Ωm, and thermal capacity of 560 J/kgK [16], making it highly suitable as a functional part and for guiding electrical currents. However, to be sure that the printing process did not significantly influence the electric resistivity and thermal capacity, two small experiments were conducted. First, the thermal capacity was measured using the same facility as previously described for the R5 test rod, and was roughly estimated as 732 ± 61 J/kgK. Note that this value may differ per 3D-printer and printer setting. Second, the electrical resistivity was measured using an electrometer (2601B, Keithley, Beaverton, OR) and was determined as 7×10^{-6} Ωm (with $R = 0.0108$ Ω, $A = 32.2$ mm^2, and $L = 50$ mm). It can be seen that the printing process (negatively) affects the thermal capacity and electric resistivity of the titanium alloy, which is most likely caused by the porosity of the titanium. Even so, the thermal capacity and electrical resistivity are still suitable for our application.

4.2 Cable Selection and Conventional Parts Manufacturing.

Next to the 3D-printed parts, some parts were manufactured or ordered, as no suitable 3D-printed alternative was available. This was the case for the steering cables, ribbons, and tension

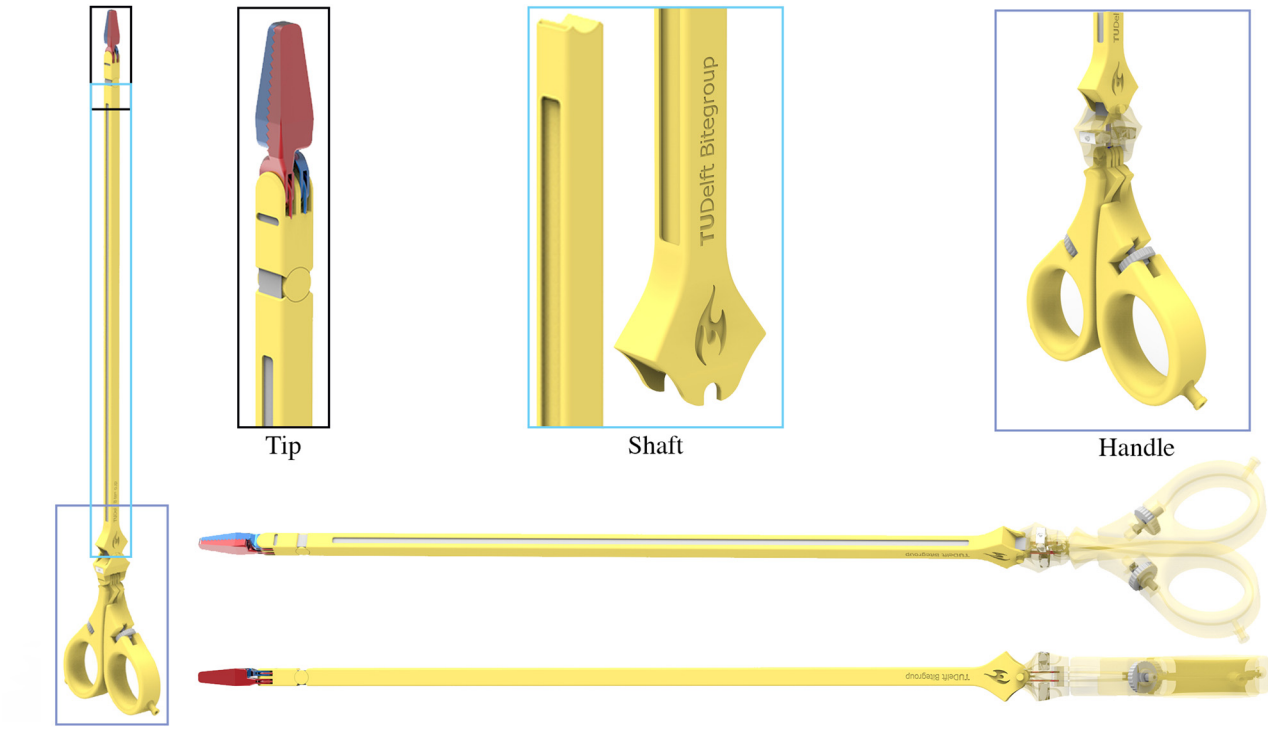

Fig. 6 Final design. The final design consists of two movable tip jaws, joint 1 to move the tip up- and downward with curve angles of ±90 deg, joint 2 to move the tip sideways (left-right) with curve angles of ±65 deg, a rectangular 5 mm shaft to guide the steering ribbons and electrode cables toward the handle, the two mirrored joints in the handle, two ring handle parts to open and close the tip jaws, two tension mechanisms to tension the electrode cables (consisting of a tension bolt and ring; situated in the handle) and steering ribbons (consisting of a rectangular box, a tension plate and M2 set screw; situated in the mirrored joint 1), 2 Ø0.45 mm electrode cables, and 2 (4 mm wide; 0.2 mm thick) polymeric steering ribbons.

Table 1 Material properties of the selected 3D-printable materials

3D-printed material	3D-printer	Material properties			
		Young's modulus E (GPa)	Ultimate tensile strength U (MPa)	Electric resistivity ϱ (Ωm)	Thermal capacity C (J/kgK)
Photopolymer R5	Perfactory 4 Standard (EnvisionTec GmbH, Gladbeck, Germany)	1.2–1.4[a]	31–39[a]	$\geq 1.67 \cdot 10^{18}$[c]	1182 ± 69[c]
Ti6Al4V	SLM 125 (ReaLizer GmbH, Borchen, Germany)	113.8[b]	950[b]	$7 \cdot 10^{-6}$[c]	732 ± 61[c]

[a]From data in Ref. [14].
[b]From data Ref. [16].
[c]Experimentally determined.

mechanisms, as 3D printing of flexible and axially stiff metals, as well as printing of miniature screw threads, is still very difficult to achieve. For the electrode cables, we decided upon using Ø0.45 mm stainless steel AISI 316 6×19 cables (*0229*, Engelmann, Hannover, Germany) [17]. These stainless steel cables are biocompatible, axially stiff with a high break load of 148 N [17], and have a low electrical resistivity of 9.4×10^{-7} Ωm (experimentally determined), making them suitable as electrode and steering cables. For the steering ribbon, it was decided to use a polymeric ribbon (0.3 mm thick, 4 mm wide). As the mechanical properties of the ribbon were unknown, a small experiment was performed in which the ribbon was fixed in a universal testing machine (*Z010*, Zwick, Venlo, The Netherlands). From this small experiment, it was determined that the ribbon has a high break load (F_{break}) of 184 ± 16.5 N ($n = 3$), an ultimate tensile strength ($\sigma_{tensile}$) of 153.3 ± 13.75 MPa ($n = 3$), a strain (ε, $n = 1$) of 2.3×10^{-4} (0.02% at 50 N) – 0.37 (37% at F_{break}), and a Young's modulus (E) of approximately 456.4 MPa ($n = 3$), making it highly suitable as a steering cable. If we compare these values with that of a similar thickness stainless steel 1×7 Ø0.3 mm cable, the ribbon has a significantly higher break load [17]. Note that no fatigue tests were performed, as the applied stress during actuation (<10 N) and minimum radius of curvature of cables and ribbon were kept under the fatigue limit (see also Jelínek et al. [12] on this topic) and the grasper is intended as a patient-specific, and thus disposable, device in the near future with a limited lifetime.

The steering ribbons and electrode cables were connected to the prototype using Pattex Instant Glue. Finally, the electrode cable and ribbon tensioning systems were manufactured using conventional manufacturing methods out of polyether ether ketone to prevent short circuits. In Fig. 7, an expanded view of the prototype is presented and in Fig. 8, the final, assembled prototype is displaced in several positions.

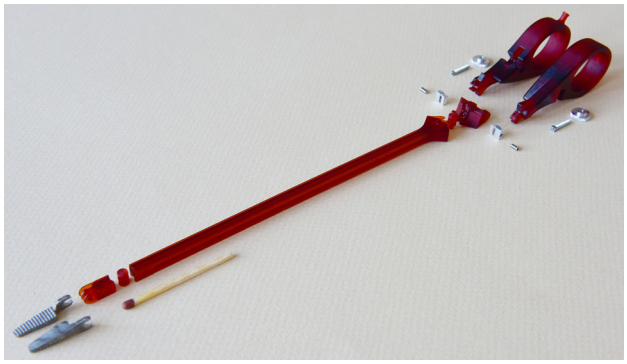

Fig. 7 Exploded view of the final prototype. The final design consists of the two titanium movable tip jaws, joint 1 to move the tip sideways (left-right) with curve angles of ±65 deg, joint 2 to move the tip up- and downward with curve angles of ±90 deg, a rectangular 5 mm shaft to guide the steering ribbons and electrode cables toward the handle, the two mirrored joints in the handle, two ring handle parts to open and close the tip jaws, two tension mechanisms to tension the electrode cables (consisting of a titanium tension bolt and ring; situated in the handle) and steering ribbons (consisting of a stainless steel rectangular box, a stainless steel tension plate and stainless steel M2 set screw; situated in the mirrored joint 1), 2 Ø0.45 mm electrode cables (biocompatible stainless steel AISI 316 1 × 7 cables [*LI000017*, Carl Stahl Technocables GmbH, Süssen, Germany]), and 2 (4 mm wide; 0.2 mm thick) polymeric steering ribbons.

5 Proof of Principle Experiment

In this section, we discuss the experiment we performed with the prototype. Two experiments were executed: in the first experiment, the movement and strength of the grasper were tested, and in the second experiment, the electrical circuit and the accompanying coagulating abilities were verified.

5.1 Dependent Variables

5.1.1 Movement and Mechanical Strength. The following dependent variables were tested:

- Output angle (deg): The output angle of both joints was measured for different input angles.
- Bending stiffness (N/mm). The bending stiffness of both joints was measured independently in a straight configuration.

5.1.2 Electrosurgical Functionalities. The following dependent variables were tested:

- Instrument temperature (°C). During activation of the electrical circuit, the temperature of the instrument was measured at various locations. A maximum instrument temperature of 40 °C was deemed acceptable to prevent unwanted tissue damage.
- Tissue temperature (°C). In this test, we evaluated how well the instrument could coagulate or destroy biological tissue. For this purpose, the tissue temperature was measured during activation of the grasper. A tissue temperature of approximately 65 °C is needed for coagulation and 100 °C for dissection purposes.

5.2 Independent Variables. The following independent variables were tested:

5.2.1 Movement and Mechanical Strength

- Input angle joint 1 (Ribbon) (deg). Input angles of 0 and 65 deg were tested for joint 1.

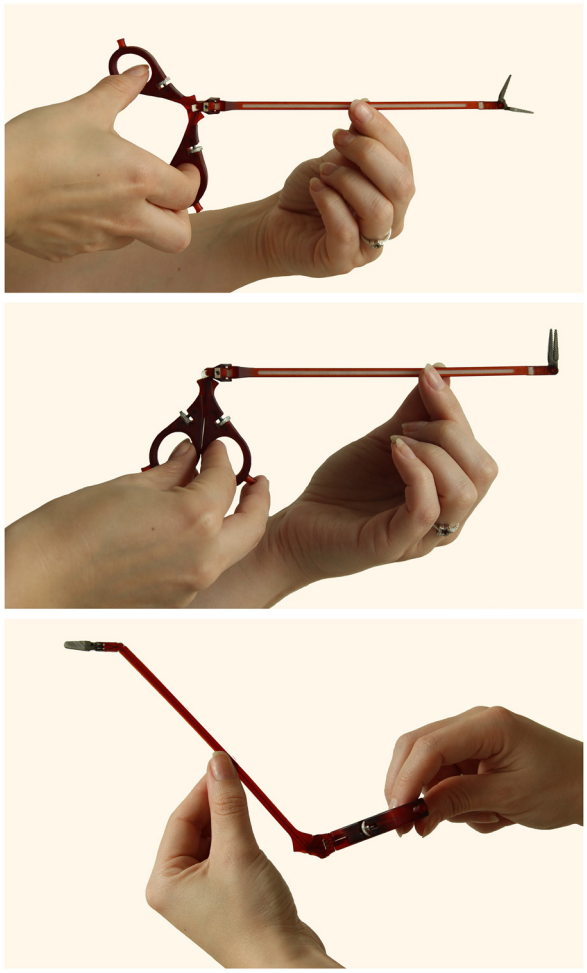

Fig. 8 Final prototype. Top: prototype with open tip jaws. Middle: prototype with joint 2 in the maximum curve angle of approximately 85 deg. Bottom: prototype with joint 1 in the maximum curve angle of 65 deg.

- Input angle joint 2 (Tip) (deg). Input angles of 0 deg and 90 deg were tested for joint 2.

5.2.2 Electrosurgical Functionalities

- Power (W). The instrument was tested at the 80 W setting of the electrosurgical unit.

5.3 Experimental Facility. The input and output angles were measured using a protractor and camera placed directly above the prototype (Fig. 9). The bending stiffness of both joints was evaluated using a universal testing machine (*LS100*, Lloyd Instruments, Bognor Regis, UK) in which the prototype was horizontally suspended (Fig. 9). For the electrosurgical functionalities test, the prototype was connected to an electrosurgical unit (*ICC300*, Erbe GmbH, Tübringen, Germany). Subsequently, the instrument and tissue temperature were measured using an infrared camera *A35* (FLIR, Wilsonville, OR). As a tissue phantom, a fresh piece of pig liver was used (Fig. 9).

5.4 Experimental Protocol. The movement and mechanical strength experiments were executed without activating the electrical circuit. The output angles were measured for all input angles (0 and 65 deg for joint 1 and 0 and 90 deg for joint 2). Each condition was tested 3 times, resulting in a total of 12 measurements. Finally, the bending stiffnesses of joints 1 and 2 were evaluated individually in the straight configuration. Again, each condition was tested 3 times, resulting in six measurements.

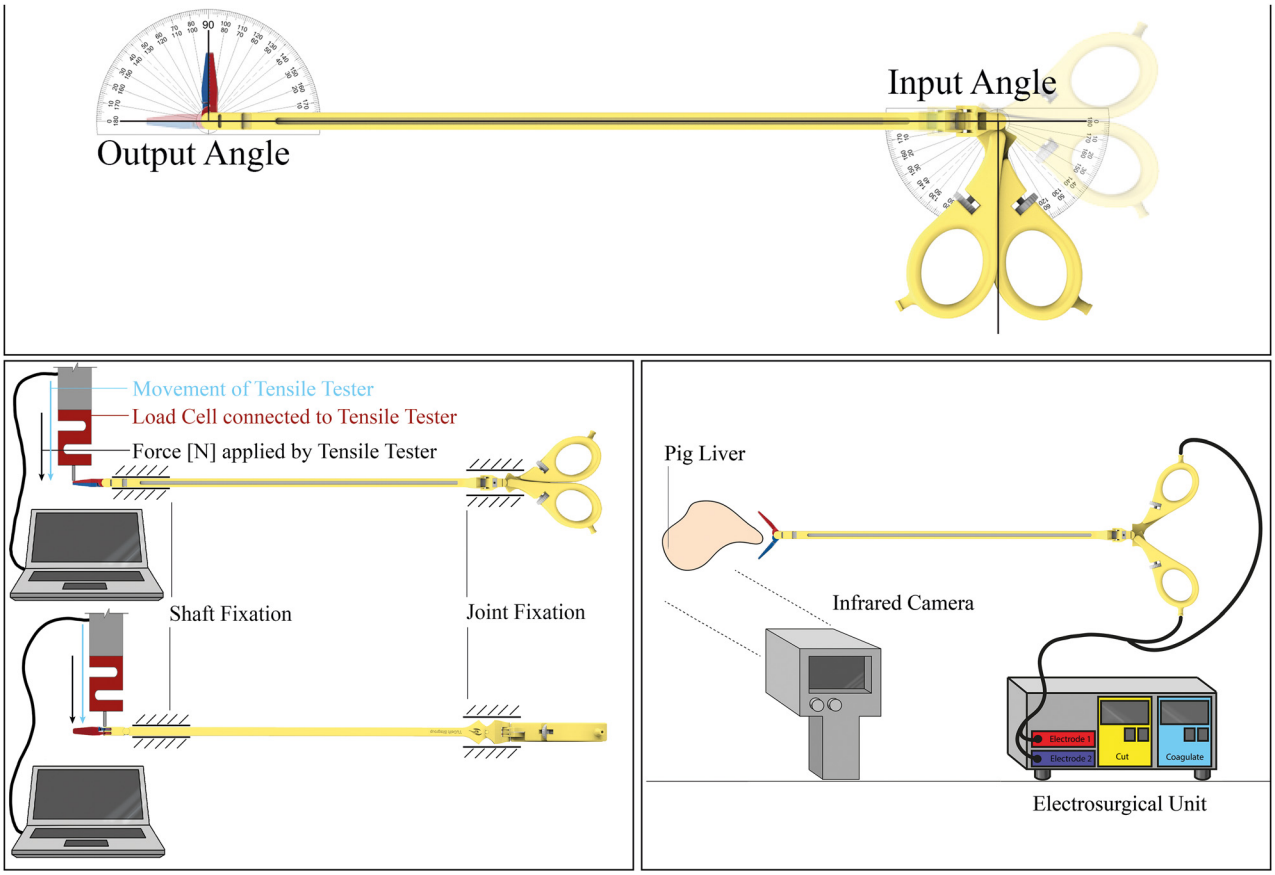

Fig. 9 Schematic representation of the experimental facility movement and mechanical strength and electrosurgical functionalities tests. Top: input–output angle measurement facility consisting of the prototype placed above two protractors and a camera to record the joint angles. Bottom left: bending stiffness measurement facility consisting of the prototype clamped horizontally in the universal testing machine (LS100, Lloyd Instruments, Bognor Regis, UK). Bottom right: the experimental facility for the electrosurgical facility test consisted of the prototype connected to an electrosurgical unit (ICC300, Erbe GmbH, Werkendam, The Netherlands), an infrared camera (*LSLT*, Optris, Berlin, Germany), and a piece of tofu or pig liver.

The electrical circuit was evaluated by measuring the temperature of the instrument and pig liver by setting the ICC300 electrosurgical unit to 80 W. A maximum activation time of 5 s was chosen. According to a study of Meeuwsen et al. [18], the average activation time of an electrosurgical tool is in between 1.4 s and 3.0 s depending on the experience of the surgeon, with a maximum of approximately 15 s. We, therefore, set the maximum activation time of our grasper at 5 s. The instrument and tissue temperatures were measured 3 times.

5.5 Data Analysis. From the input and output angle data, the energy losses from handle to tip were calculated. The data from the universal testing machine were processed using Microsoft Excel to determine the bending stiffness of the joint.

For the electrosurgical functionalities experiment, the data from the infrared camera A35 were read out using PLEORA GEV software (Pleora Technologies, Ottawa, ON, Canada) and a program was written to visualize and analyze the tissue temperature over time.

6 Results and Discussion

6.1 Movement and Mechanical Strength. The proposed bipolar steerable grasper increased the workspace of currently available rigid bipolar graspers. The addition of the joint allows the tip orientation to be controlled, making it possible to reach around structures that would otherwise obstruct the surgery. The instrument can be easily maneuvered and controlled using the ring handles, resulting in a smooth movement of the tip joints. The low steering forces are a result of the design of the joints in which the steering ribbons and cables are placed at the outer edge of the joint to maximize the moment arms. Furthermore, as the ribbon has a very low thickness and is made from braided polymer strands, the bending stiffness is low, again, decreasing the steering forces. The tip of the instrument follows the movement of the handle of the instrument nicely with minimal energy loss, reaching an output angle of 65 deg for joint 1 and 85 deg for joint 2 (5.6% energy loss). The minimal energy loss is, again, most likely due to the design of the joints, which minimizes steering forces and thus elongation of the steering ribbons and cables. The grasper does illustrate some hysteresis, mainly due to the friction of the cylindrical joint and ribbons with the shaft. However, we feel that this can be minimized by material choice and adding a (dry) lubricant. The bending stiffness was on average 4.0 N/mm (0.7 N/ deg or $7.9{\cdot}10^{-2}$ N·m/deg) for joint 1 (ribbon; $n = 3$; range 3.35–4.48;) and 4.4 N/mm (1.5 N/ deg or $2.9{\cdot}10^{-2}$ N·m/ deg) for joint 2 (tip; $n = 3$; range 3.43–5.14). When compared to the currently available steerable instruments investigated in the study of Jelínek et al. [8], the bending stiffness of the developed instrument is between 1.4 and 7.8x higher than the currently available tools in the straight configuration, which allows for high precision steering and support during the procedure. The reason for this high bending stiffness is the unique joint design. Both joints allow for only 1DOF radially rotating motion (planar) and restrict axial rotation and shortening (energy storage). Furthermore, due to the maximized moment arms, the joint diameter could be maximized, thus

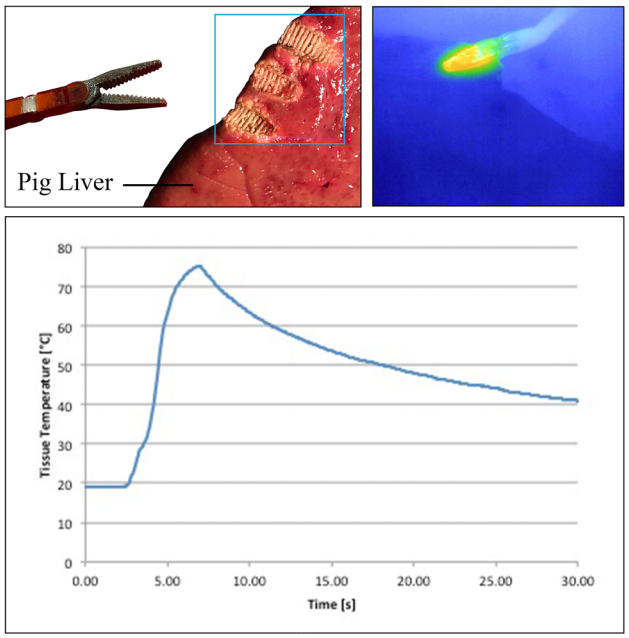

Fig. 10 Electrosurgical grasper coagulating a piece of pig liver. Left: the electrosurgical grasper with pieces of coagulated pig liver (see the cyan rectangle). Middle: infrared image of the grasper during coagulation. Right: graph of the tissue temperature over the time. The temperature of the pig liver reached approximately 75 °C with an activation time of only 5 s, coagulating and desiccating the liver between the tip jaws. The power was set to 80 W.

reducing the influence of residual (radial) forces. Finally, the use of the ribbon maximized the cross-sectional area, while not negatively affecting the moment arms, which resulted in an increase of the bending stiffness.

6.2 Electrosurgical Functionalities. The ability to effectively coagulate tissues to stop excessive bleeding during surgery is a necessity for many surgical procedures. In a proof-of-principle experiment, the grasper demonstrated the ability to safely guide an electrical current from the handle to the tip in order to coagulate and destroy tissue in direct contact with the movable jaws (see Fig. 10), with a maximum measured tissue temperature of 75 °C for an activation time of only 5 s. The instrument temperature stayed well below 40 °C due to the large cross-sectional area and low electric resistance of the looped electrode cables, except from the tip, which reached approximately 60 °C. The tip of the grasper increased in temperature due to the increased resistance introduced by the 3D-printing process. An improved printing process can potentially minimize this tip heating effect in the near future. Additionally, an extra isolating layer may be added to the tip jaws.

6.3 Current Limitations of 3D-Printing. We have illustrated the ability to 3D-print a steerable electrosurgical grasper for use in MIS. During this process, it became apparent that even though we have made huge progress in the last 10 years with 3D-printing technology, there are still some limitations that need to be overcome (see also Appendix). Mainly, with respect to metal 3D-printing, some challenges need to be overcome in order to allow for manufacturing of small functional parts. As of today, no suitable 3D-printing process exists that provides a similar mechanical strength and behavior to off-the-shelf cables and ribbons. Moreover, printing of functional parts or components, such as screw threads, is also challenging, especially on a miniature scale. It was also seen that the 3D-printing process can negatively affect the electrical properties of the material, resulting in the higher electric resistivity of the 3D-printed titanium compared to conventionally manufactured titanium (7×10^{-6} Ωm versus 1.8×10^{-6} Ωm, respectively), most likely caused by pores in the material. Even though 3D printing is still not suitable for large-scale manufacturing of MIS instruments, they are rapidly developing. 3D-printers are becoming faster and cheaper, while simultaneously allowing for printing smaller parts at higher resolutions. Together with the versatility of 3D printing, we, therefore, feel that in the near future, many implants and MIS instruments will be manufactured using this technique.

6.4 Future Steps and Recommendations. The proposed grasper demonstrated the ability to change the position of the tip relative to the shaft and to coagulate tissues, using only 20 parts. Future developments of this instrument should be focused on exploring different 3D-printed materials and configurations of joint placement, shaft shapes, tip configurations, and handle designs. The location and shape of the connector could be optimized to allow for easy operation and connecting to the electrosurgical unit. Furthermore, in order to manufacture patient-specific tools in the near future, pre-operative data, such as data from a chronic total occlusion or magnetic resonance imaging scan, should be fed into 3D-CAD modeling software to calculate the most optimal shape. This 3D-CAD model could, subsequently, be 3D-printed and assembled prior to the procedure, allowing for patient-specific instruments that will benefit both the patients and surgeons by improving the fit of implants and allowing for safely navigating through tight spaces, among others.

7 Conclusions

This study presents the design and validation of the first adaptable and steerable 3D-printed bipolar electrosurgical grasper (□ 5 mm shaft cross section). The addition of a steering segment significantly increases the reach of the tool, whereas the 3D-printed fabrication protocol means that the design of the instrument is both versatile and adaptable. The instrument provides 2DOF over two joints with a curve angle of ±65 deg for sideways (left–right) movement (actuated by two polymeric steering ribbons that are 0.3 mm thick and 4 mm wide and ±85 deg for up- and downward movement (actuated by two Ø0.45 mm electrode cables). The joints have a significantly higher bending stiffness (by a factor of between 1.4 and 7.8x) than currently available steerable instruments, mainly due to the placement of the cables and ribbons at the outer edge of the instrument and the joint geometry, which restricts axial rotation and translation. The tip jaws can be opened and closed with angles up to 170 deg and can be used to coagulate tissues in between the jaws as they are connected to the two electrode cables that both actuate the bending motion and guide electrical current from the handle toward the tip. In the handle, the two 1DOF planar joints are mirrored and the tip jaws are replaced by a ring handle (similar to the handle of a pair of scissors) to control the tip joints and opening and closing of the movable jaws. Furthermore, in the ring handles, an electrode cable tension mechanism was integrated to keep the cables and joints under tension, and an electrode connector was added to connect an electrosurgical unit to the device. The instrument requires very little steering forces and has demonstrated the ability to coagulate soft tissues, with measured tissue temperatures of 75 °C for an activation time of only 5 s. This 3D-printed instrument is the first in its class and opens up future opportunities for patient-specific surgery with a considerably higher reach than the rigid instruments currently available.

Acknowledgment

We would like to thank Menno Lageweg, Remi van Starkenburg, Sander Leeflang, Wim Velt, and Zjenja Doubrovski for their contribution in the development and manufacturing of the prototype. Additionally, we would like to thank Arjan van Dijke, Jos

van Driel, Martijn Tijssen, Rob Luttjeboer, Rowland de Roode, Stefaan Heirman, and Ton Riemslag for their help in the design and set-up of the measurement facilities.

Funding Data

- Dutch Technology Foundation TTW, The Netherlands Organization for Scientific Research (NWO).
- The Ministry of Economic Affairs.
- Stichting voor de Technische Wetenschappen (12710).

Nomenclature

A = cross-sectional area (m^2)
C = heat capacity (J/kgK)
DOF = degrees-of-freedom
F = load applied to the system (N)
F_{break} = load at which the material breaks (N)
3D = three-dimensional
L = length (m)
m = mass (kg)
MIS = minimal invasive surgery
Q = added heat (J)
R = electrical resistance (Ω)
ΔT = change in temperature (K)
δ = deflection (mm)
ε = strain (…)
$\sigma_{tensile}$ = tensile stress (N/m^2)
ϱ = electrical resistivity (Ωm)

Appendix: Joint Selection Process

In this section, we will discuss the fundamental joint categorization and the selection process of the final joint design based on the printability, joint requirements, and bipolar requirements.

A.1 Fundamental Joint Categorization. The main challenge of designing a steerable electrosurgical tool is to achieve a reliable and safe way of guiding the current through or around the joint. For this purpose, we have made a fundamental categorization of joint types and ways of guiding the electrical current through or around the joint (Fig. 11). A first subdivision is based on geometrical properties of the joints (Fig. 11). The first group consists of joints made from a single component (*one-piece (compliant) joint*). These joints depend purely on the dimensions of the flexural part enabling the bending and the joint's material properties, such as stiffness or yield strength. Since the joint is formed of a single piece and operates within the range of the material's elastic deformation, it essentially acts as a spring. An example of such a joint is a leaf spring. The second group consists of joints made from more than one component (*multipiece joint*). These joints rely on either high enough friction between the moving parts in rolling joints, or relatively low friction in sliding joints, to transfer the motion.

A second subdivision is based on how the current flows through the joint (Fig. 11). The *one-piece* and multipiece joint groups are each divided into three groups: *completely conducting*, *partially conducting*, and *nonconducting* joints. In the completely conducting group, the joint itself is made entirely out of conducting material. The joint structure effectively doubles as the electrode. Since the entire joint is conductive, an outer insulating layer is needed to prevent any current from entering the body other than at the tip of the instrument (Fig. 11). In the partially conducting group, the joint is made from two different materials: a conducting and a nonconducting material. In this group, the electrode is embedded into the joint and is printed in the same cycle as the nonconducting component to create a single part. Finally, in the nonconducting group, the joint itself is made entirely from nonconducting material; separate electrodes are needed to guide the electricity through the joint. The key difference between the partially conducting and nonconducting group is that the electrode in the partially conducting group are embedded inside the joint and cannot be removed, whereas the electrodes in the nonconducting group are inserted into the joint after manufacturing in an assembly stage.

Within the nonconducting group, a second distinction can be made between *externally placed electrodes* and *internally placed electrodes*. The externally placed electrodes are guided around the joint, necessitating an insulating layer (Fig. 3) to prevent any current from entering the body, whereas the internally placed electrodes are guided through the joint itself and thus do not require an insulating layer (Fig. 11). It is, however, advisable to use an insulating layer (or sealing) as current leakage (as a result of insulation failure) is thought to be responsible for most injuries caused during electrosurgery [19].

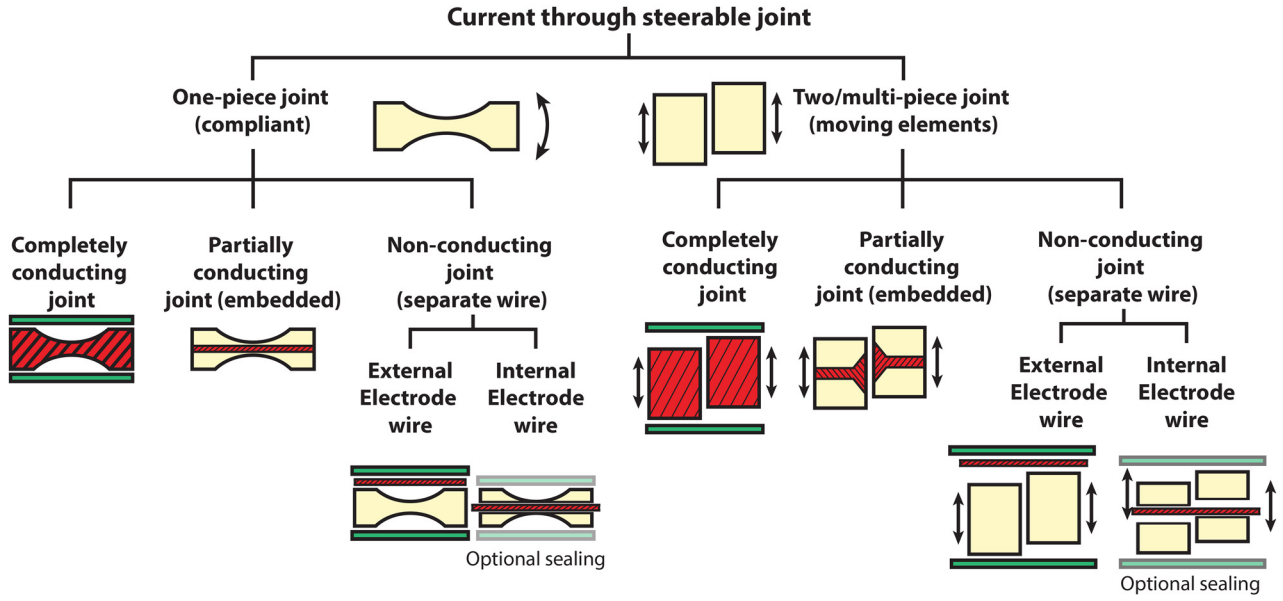

Fig. 11 Fundamental joint categorization. The conductive material is indicated with dashed surfaces. The insulating material is indicated with the lightly shaded surfaces. The sealing is indicated with the darkly shaded rectangular surfaces.

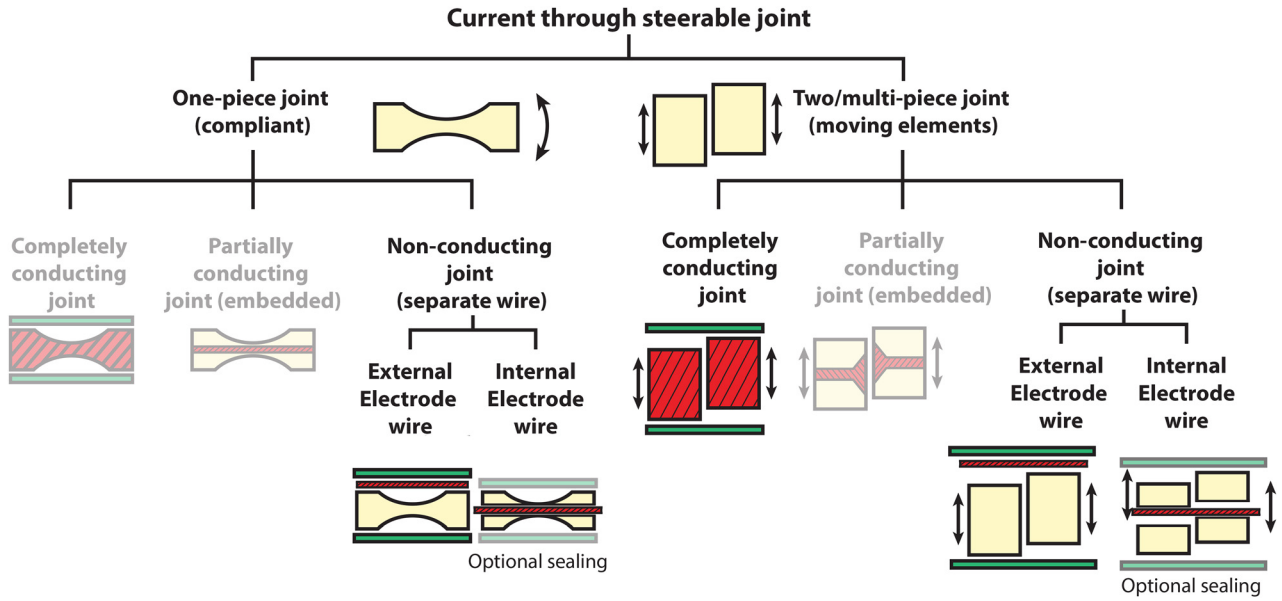

Fig. 12 Fundamental joint categorization based on printability. The *one-piece completely conducting joint*, *one-piece partially conducting joint*, and multipiece partially conducting joint are eliminated as flexible conducting materials are currently not available for 3D-printing and multimaterial printing is still limited. The conductive material is indicated by the dashed surfaces. The insulating material is indicated by the lightly shaded surfaces. The sealing is indicated by the darkly shaded slender rectangular surfaces at the outer edges of the joint.

A.2 Joint Selection Process

A.2.1 Elimination Based on Printability. Although 3D printing of polymers has come a long way since it was first introduced in 1981 (by Hideo Kodama [20]), 3D printing of high-precision structural metal parts has not yet come as far. The main consequence this will have for us is that it is not possible *yet* to print flexible conducting materials (metals). As can be seen from Fig. 11, four joint groups rely on flexible (conducting) components. However, only two of those groups rely on flexible conducting components that have been 3D-printed; the *one-piece (compliant) completely conducting joint* group and *one-piece (compliant) partially conducting joint* group. Since we cannot make such components with current technologies, these two groups will be eliminated. Furthermore, for the *multipiece partially conducting joint* group, a multimaterial printer is needed. Unfortunately, 3D-printers that can print multiple materials, specifically metallic and polymeric materials, in one cycle, are not readily available. Therefore, the multipiece partially conducting joint group is also eliminated. This leaves us with the *one-piece nonconducting joint, multipiece completely conducting joint*, and *multipiece nonconducting joint* groups (Fig. 12).

A.2.2 Elimination Based on Joint Requirements. Joints can be fundamentally divided into *planar*, *universal*, and *spherical joints*. In Fig. 13, schematic representations of these joints for the one-piece and *multipiece* configurations are given. A *planar joint* allows for one rotational DOF, resulting in a two-dimensional

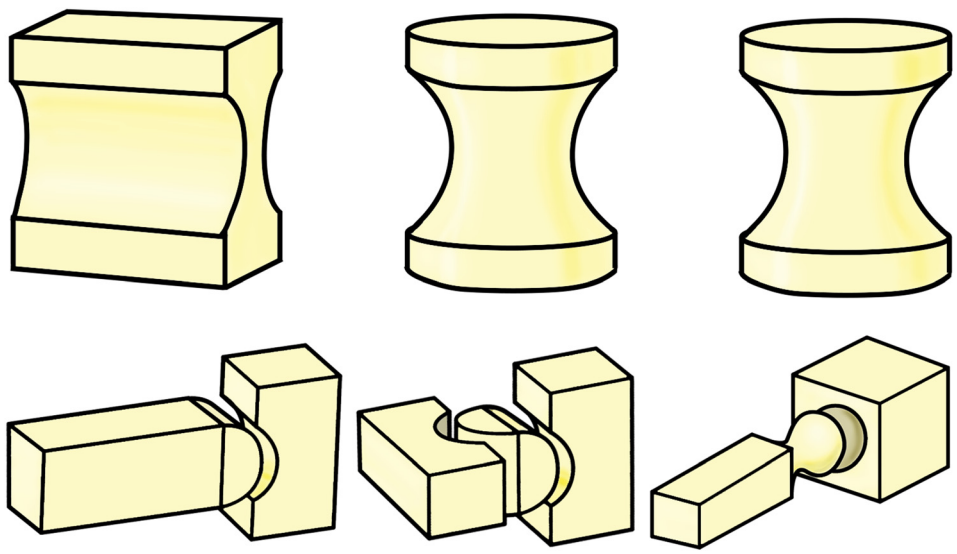

Fig. 13 Fundamental joint design. Top left: one-piece (compliant) planar joint. Top Middle: one-piece (compliant) universal joint. Top right: one-piece (compliant) spherical joint. Bottom left: multipiece planar joint. Bottom middle: multipiece universal joint. Bottom right: multipiece spherical joint.

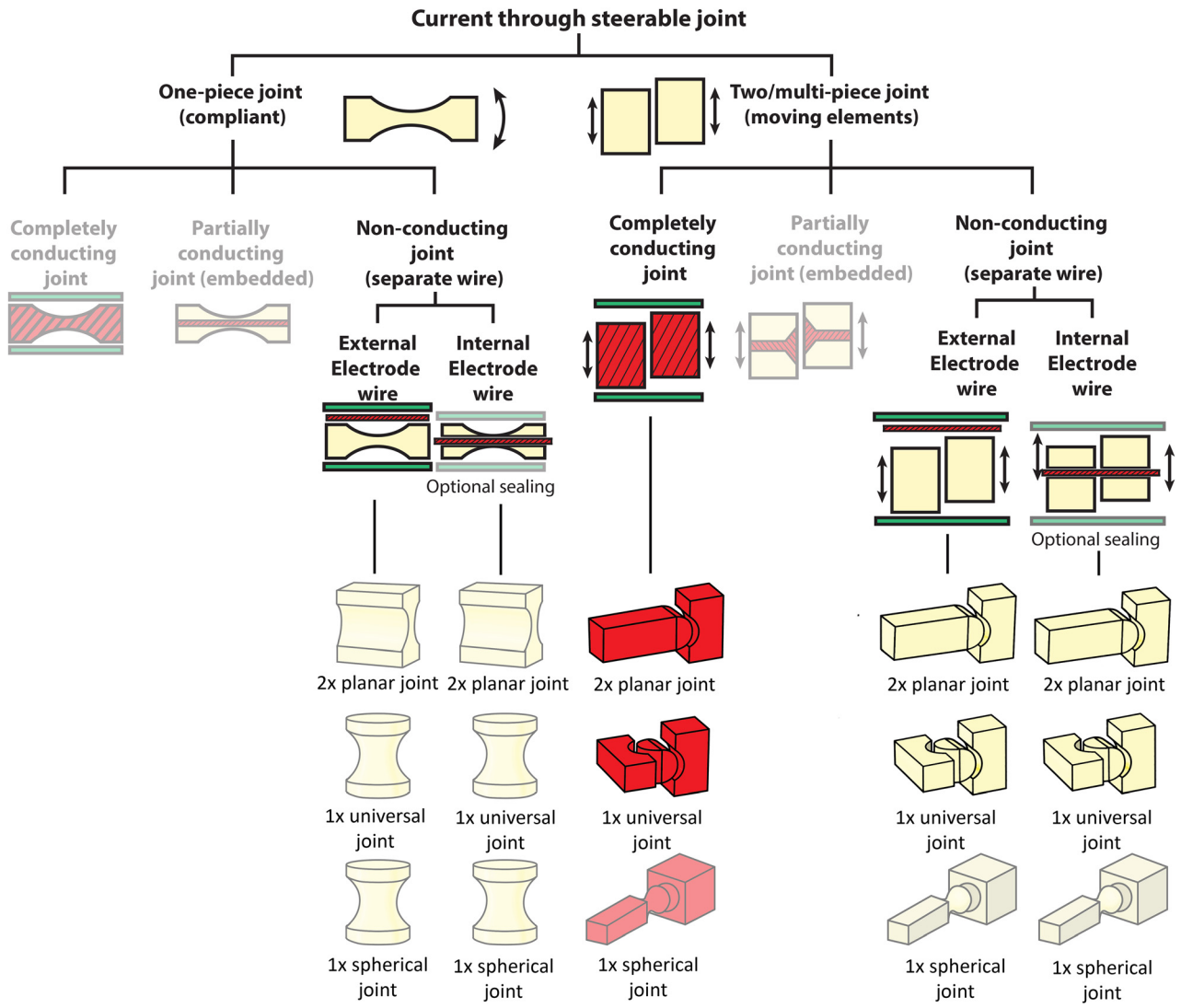

Fig. 14 Fundamental joint categorization based on printability and design requirements. The conductive material is indicated by the (dashed) darkly shaded surfaces. The insulating material is indicated by the lightly shaded surfaces. The sealing is indicated by the darkly shaded rectangular surfaces at the outer edges of the joints.

circular workspace. An example of such a joint is a leaf spring (one-piece) or hinge joint (multipiece). The *universal joint* allows for two rotational DOFs, resulting in a three-dimensional spherical workspace. Finally, spherical joints allow for three rotational DOF. An example of a *multipiece spherical joint* is a ball and socket joint.

By looking at the joint requirements and wishes for our instrument, we can eliminate several groups from our joint designs. As previously discussed, the joint should allow for 2DOF bending motion. For planar joints, this can only be achieved by placing two joints in sequence. The universal and spherical joint allow for 2 and 3DOF motions, respectively. Another requirement is that the joint should be torsional stiff. This eliminates the spherical joint, since this allows for axial rotation and is thus not torsional stiff. Furthermore, when taking a step back to the fundamental joint categorization scheme in Fig. 11, it becomes clear that a torsional stiff 2 DOF *nonconducting one-piece joint* is not possible as a single flexible joint with 2 DOF results in a narrow joint design as shown in Fig. 13. Even though it is possible to create a semistiff onepiece nonconducting joint by placing two planar joints in sequence, the flexibility (or compliancy) requirement of this joint design (and thus the used material) enables some axial rotation. Furthermore, such a joint requires a continuous force to keep it in a bent state, as it always tries to return to its neutral, straight, state, and, if allowed, the joint may overstretch thus introducing plastic deformation, after which the joint will not return to its straight neutral position. Therefore, this joint group is eliminated. Now only four main groups remain (Fig. 14): *multipiece completely conducting planar joint (2x)*, *multipiece completely conducting universal joint*, *multipiece nonconducting planar joint (2x)*, and *multipiece nonconducting universal joint*.

A.2.3 Elimination Based on Bipolar Requirements. In Secs. A.1, A.2.1, and A.2.2, we assumed a simple one-way current through the joint (monopolar). However, in a bipolar electrosurgical instrument, two separate current paths should be guided through the joint: one active and one return electrode. Therefore, in this section, we will create a bipolar representation of the multipiece completely conducting universal joint, multipiece completely conducting planar joint (2*x*), *multipiece nonconduction universal joint*, and *multipiece nonconduction planar joint (2x)* (Fig. 15). To make the multipiece completely conducting universal joint and *planar joint (2x)* suitable for a bipolar application, it is a necessity to add an insulating layer in the joint to separate the active and return electrode (see Fig. 15). As previously discussed, a multimaterial 3D-printer that can print metallic and polymeric

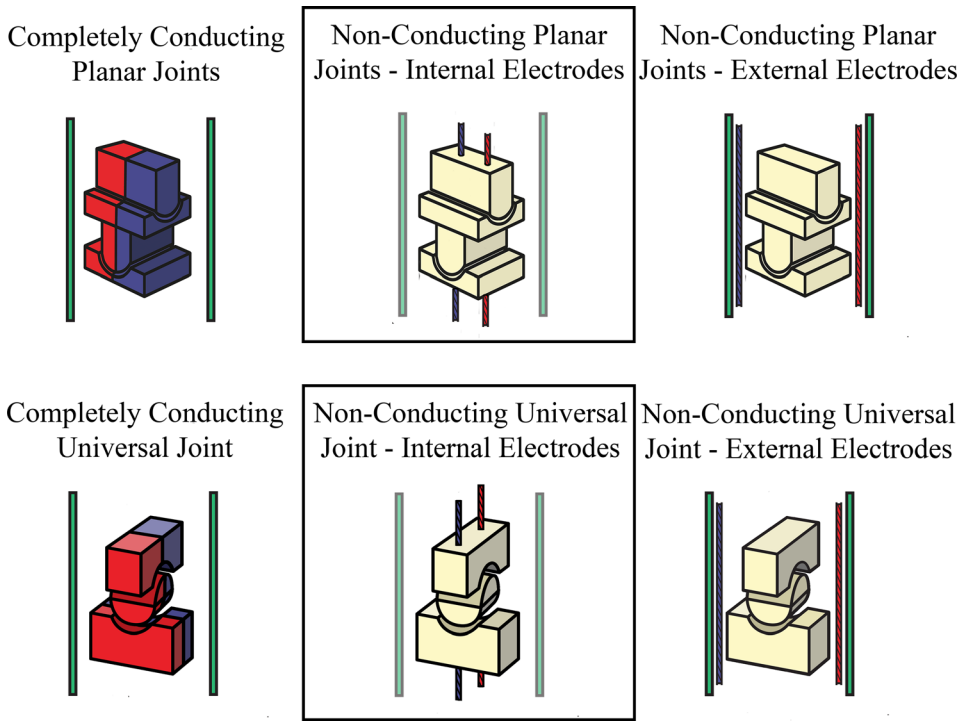

Fig. 15 Bipolar versions of the Joint designs. Top row from left to right: multipiece completely conducting planar joint (2*x*), *multipiece nonconducting planar joint (2x) with internal electrodes*, and *multipiece nonconducting planar joint (2x) with external electrodes.* Bottom row from left to right: multipiece completely conducting universal joint, *multipiece nonconducting universal joint with internal electrodes*, and *multipiece nonconducting universal joint with external electrodes*. Due to the inability to print the multipiece completely conducting joints and the preference that the electrode cables are guided through the instrument, the multipiece nonconducting joints with internal electrodes will be developed further (indicated by the black rectangular boxes). The conductive material is indicated by the darkly shaded surfaces. The insulating material is indicated by the lightly shaded surfaces. The sealing is indicated by the darkly shaded slender rectangular surfaces at the outer edges of the joints. The completely conducting joints are subdivided into an active and return electrode. In the nonconducting joints, the active and return electrode are indicated with the dashed slender rectangular surfaces.

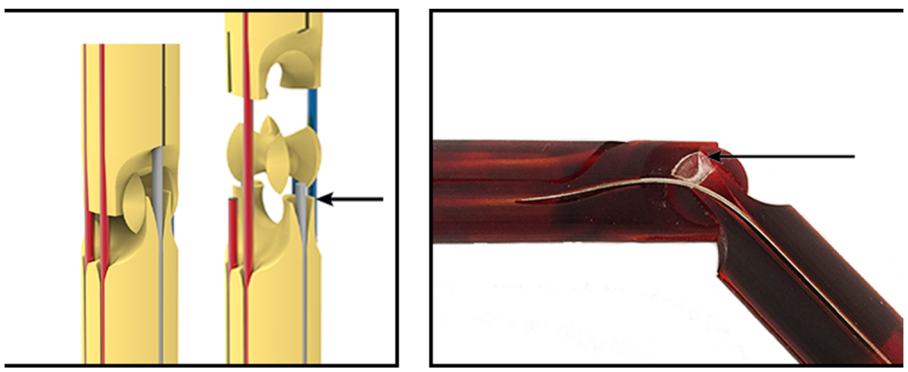

Fig. 16 Scaled prototype multipiece nonconduction universal joint. Left: renderings of the multipiece nonconduction universal joint consisting of two "shafts" with rounded cylindrical recesses and a spherical cross. Right: scaled (3*x*) printed prototype. The arrow indicates the weakest part of the prototype, which, when printed on a 5 mm scale, will be too weak. Therefore, this design was eliminated.

elements in one cycle is not readily available. Therefore, this category is eliminated. For the bipolar configuration of the multipiece nonconduction universal joint and planar joint, two different configurations need to be taken into account; one with *external electrodes* and one with *internal electrodes* (Fig. 15). To make the multipiece nonconduction universal joint and planar joint suitable for bipolar application, it is a necessity to add one or more electrode cables to the joint that will make up the active and return electrode, respectively.

For the external electrode category, the electrode cables need to be insulated, both from each other and the environment, whereas external insulation is no issue in the internal electrode category.

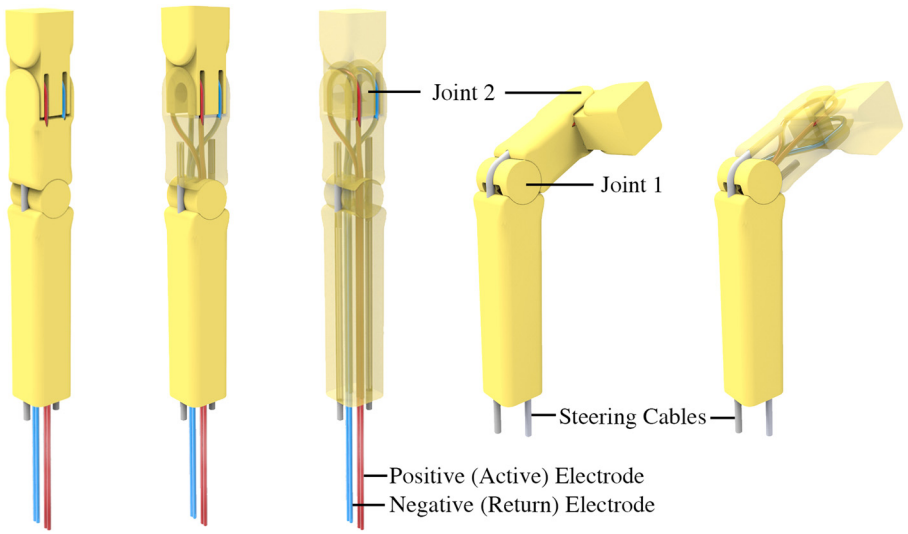

Fig. 17 Conceptual one-piece nonconduction planar joint design

Therefore, the internal electrode category is preferred.

Based on the discussed pros and cons of the bipolar representation of the given joint categories, only two joint designs remain: multipiece nonconduction universal joint and multipiece nonconduction planar joint (2*x*), both with internal electrodes. To test the feasibility of these designs, two scaled (2*x*) prototypes were manufactured using a Perfactory 4 Standard (EnvisionTec, Dearborn, MI) 3D printer. From these prototypes, it became clear that the multipiece nonconduction universal joint would be too weak and fragile when printed on a 5 mm scale (Fig. 16). We, therefore, decided to eliminate this category. In Sec. A.2.4, the multipiece nonconduction planar joint (2*x*) with internal electrode will be developed further.

A.2.4 Conceptual Joint Design. In Fig. 17, a schematic drawing of the conceptual joint design is given. As can be seen from Fig. 17, the design contains a square shaft and two serially placed planar joints. The main benefit of using a square shaft over a circular shaft is that the planar joints can be maximized in size and thus in strength. The first planar joint moves the instrument left and right with a curve angle of 130 deg (65 deg in each direction) and consists of a large cylindrical barrel that is confined (on two sides) by a semicylindrical recess in the shaft (Fig. 17). Two steering cables located at the circumference of the barrel actuate the joint (Fig. 17). To prevent cable kinking during bending, the barrel contains two hourglass shaped lumina. The second (more distal) planar joint moves the tip upward and downward with a curve angle of 180 deg (90 deg in both directions) and consists of a (open) hinge joint in which the tip section contains a semicylindrical groove that clicks upon a fixed axle (Fig. 17). To steer the joint and to guide electricity to the tip, two Ø0.5 mm cables are used, which are guided through two separate lumens in the center of the first joint and are looped around two separate circular grooves in the tip section (Fig. 17). By tensioning the cables, friction between the cables and grooves will keep the cable in place during movement. However, for safety, a small hole is present at the apex of the circular grooves through which glue can be applied to fix the cables in place. From here, they follow the same path back to the handle of the instrument. By creating a loop at the end of the cables, the effective diameter of the cables is doubled, allowing for higher forces that can be exerted on the tip portion. Furthermore, by using a looped cable that bypasses both joints, the chance of electrical interruptions (by loose connections or contacts) and the risk of cable loosening are minimized.

A.3 Joint Optimization Process

A.3.1 From Cables to a Ribbon. In most steerable instruments, two cables are used to control 1DOF, one for each direction. The required cross-sectional area (or size) of the steering cables is dependent on the required force to bend the joint and the bending stiffness of the cable itself. Instead of 2 cables to control 1 DOF, it is, therefore, also possible to use several smaller cables or even a rectangular ribbon with an equal cross-sectional area. The use of a ribbon to control the joint has two main advantages. First, the wires can be placed very close to the edge of the joint, increasing the moment arm of the cables and thus reducing the required force for bending, as well as increasing the joint size and bending stiffness of the joint (Fig. 18). Furthermore, the increase in joint size increases its stability, allows for the incorporation of thicker internal electrode cables, and allows for it to function as a guidance structure for the cable ribbon during bending motions. The second advantage is the bending radius these wires can accommodate. As a rule of thumb, the bending radius of a cable should not be lower than 5x its diameter to prevent cable fatigue. By minimizing the cable thickness, smaller radii can be navigated.

A.3.2 Tip and Joint Integration. The distance between the tip (with the movable jaws) and the joints should be as small as possible to allow for direct steering and precise tip positioning. In

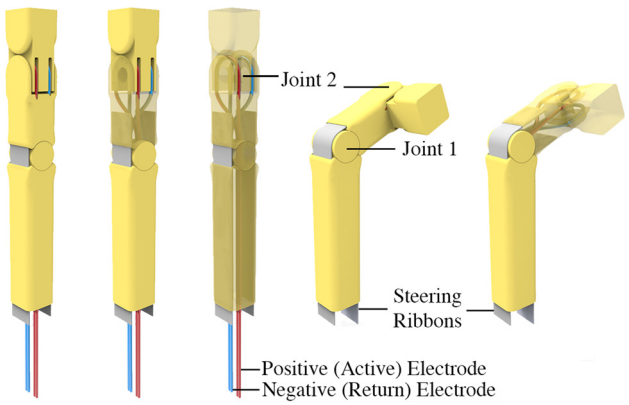

Fig. 18 Optimization of the one-piece nonconduction planar joint design; from cables to a ribbon

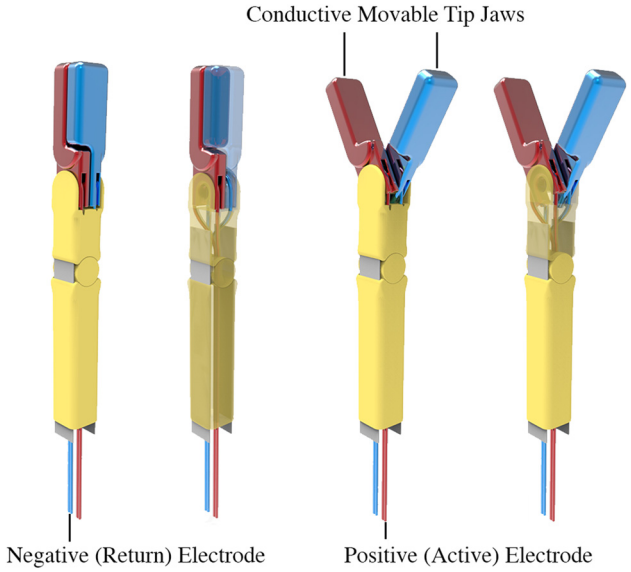

Fig. 19 Optimization of the one-piece nonconduction planar joint design: tip and joint integration

order to minimize the distance between the tip and joints, it was decided to integrate the tip section with the second planar joint. For this purpose, the shaft distally to the second joint was cut through the midline, giving to (basic) separate tip jaws (Fig. 19). To each of the jaws, one of the electrode cables is connected. As such, the second (distal) planar joint and the connected electrode cables enable the rotation of the entire tip, as well as the opening and closing of the jaws (Fig. 19).

References

[1] Taheri, A., Mansoori, P., Sandoval, L. F., Feldman, S. R., Pearce, D., and Williford, P. M., 2014, "Electrosurgery—Part I: Basics and Principles," J. Am. Acad. Dermatol., **70**(4), p. 591.

[2] Ethicon U.S. LLC, 2017, "Ethicon Laparoscopic Hand Instruments," Ethicon U.S. LLC, Somerville, NJ, accessed May 1, 2017, http://www.ethicon.com/healthcare-professionals/products/other/lap-hand/laparoscopic-hand-instruments

[3] Aesculap AG, 2016, "Aesculap AdTec Bipolar: The Blue (R)Evolution," Aesculap AG, Tuttlingen, Germany, accessed May 1, 2017, http://itmedica.com/wp-content/uploads/2017/01/ADTEC_BIPOLAR.pdf

[4] Intuitive Surgical, 2017, "EndoWrist Instruments," Intuitive Surgical, Sunnyvale, CA, accessed Aug. 24, 2017, https://www.intuitivesurgical.com/products/instruments/

[5] Stryker, 2017, "Stryker Reliability for All Laparoscopic Procedures," Stryker, Kalamazoo, MI, accessed May 1, 2017, http://www.stryker.com/stellent/groups/public/documents/web_content/126639.pdf

[6] Toledo, L., Gossot, D., Fritsch, S., Revillon, Y., and Reboulet, C., 1998, "Study of Sustained Forces and the Working Space of Endoscopic Surgery Instruments," Ann. Chir., **53**(7), pp. 587–597.

[7] Leijendeckers, P., Fortuin, J., Herwijnen, F., and Schwippert, G., 2003, *Polytechnisch Zakboek*, Elsevier Bedrijfsinformatie B.V., Arnhem, The Netherlands.

[8] Jelínek, F., Gerboni, G., Henselmans, P. W. J., Pessers, R., and Breedveld, P., 2015, "Attaining High Bending Stiffness by Full Actuation in Steerable Minimally Invasive Surgical Instruments," J. Minimally Invasive Ther. Allied Technol., **24**(2), pp. 77–85.

[9] Aesculap, 2012, "Aesculapusa Laparoscopic Instruments Overview," Aesculap, Center Valley, PA, accessed May 1, 2017, https://www.aesculapusa.com/assets/base/doc/DOC960-Laparoscopic_Instruments_Overview_Brochure.pdf

[10] Stryker, 2017, "Stryker Laparoscopic Instruments," Stryker, Kalamazoo, MI, accessed May 1, 2017, http://www.stryker.com/en-us/products/Endoscopy/LaparoscopyLaparoscopicInstruments/LaparoscopicInstruments/index.htm

[11] Alkatout, I., Schollmeyer, T., Hawaldar, N. A., Sharma, N., and Mettler, L., 2012, "Principles and Safety Measures of Electrosurgery in Laparoscopy," JSLS, **16**(1), pp. 130–139.

[12] Jelínek, F., Pessers, R., and Breedveld, P., 2014, "DragonFlex Smart Steerable Laparoscopic Instrument," ASME J. Med. Devices, **8**(1), p. 015001.

[13] EnvisionTec, 2017, "EnvisionTec Perfactory Family P4 Standard," EnvisionTec, Gladbeck, Germany, accessed May 1, 2017, https://envisiontec.com/3d-printers/perfactory-family/perfactory-4-standard/

[14] EnvisionTec, 2017, "EnvisionTec Perfactory Materials R5," EnvisionTec, Gladbeck, Germany, accessed May 1, 2017, https://envisiontec.com/3d-printing-materials/perfactory-materials/r5/

[15] Realizer, 2017, "Realizer SLM 125," Realizer, Borchen, Germany, accessed May 1, 2017, http://www.realizer.com/?page_id=2107

[16] ASM, 2017, "ASM Titanium Ti-6Al-4V (Grade 5), Annealed," ASM Aerospace Specification Metals, Inc., Pompano Beach, FL, accessed May 1, 2017, http://asm.matweb.com/search/SpecificMaterial.asp?bassnum=mtp641

[17] Engelmann vom Hoven Group, 2017, "Engelman Broschüre Feinseile," Engelmann vom Hoven Group, Hannover, Germany, accessed May 1, 2017, https://engelmann-online.de/wp-content/uploads/2015/09/Broschuere_Feinseile_DE_web.pdf

[18] Meeuwsen, F. C., Guédon, A. C. P., Arkenbout, E. A., van der Elst, M., Dankelman, J., and van den Dobbelsteen, J. J., 2017, "The Art of Electrosurgery: Trainees and Experts," Surg. Innovation, **24**(4), pp. 373–378.

[19] Montero, P. N., Robinson, T. N., Weaver, J. S., and Stiegmann, G. V., 2010, "Insulation Failure in Laparoscopic Instruments," Surg. Endoscopy, **24**(2), pp. 462–465.

[20] Kodama, H., 1981, "Automatic Method for Fabricating a Three-Dimensional Plastic Model With Photo-Hardening Polymer," Rev. Sci. Instrum., **52**(11), pp. 1770–1773.